

# Comprehensive constraints on a spin-3/2 singlet particle as a dark matter candidate

Ran Ding <sup>a,\*</sup> Yi Liao <sup>a,†</sup> Ji-Yuan Liu <sup>b,‡</sup> and Kai Wang <sup>c,§</sup>

<sup>a</sup> *School of Physics, Nankai University, Tianjin 300071, China*

<sup>b</sup> *College of Science, Tianjin University of Technology, Tianjin 300384, China*

<sup>c</sup> *Zhejiang Institute of Modern Physics and Department of Physics,  
Zhejiang University, Hangzhou, Zhejiang 310027, China*

## Abstract

We consider the proposal that dark matter (DM) is composed of a spin-3/2 particle that is a singlet of the standard model (SM). Its leading effective interactions with ordinary matter involve a pair of their fields and a pair of SM fermions, in the form of products of chiral currents. We make a comprehensive analysis on possible phenomenological effects of the interactions in various experiments and observations. These include collider searches for monojet plus missing transverse energy events, direct detections of DM scattering off nuclei, possible impacts on the gamma rays and antiproton-to-proton flux ratio in cosmic rays, and the observed relic density. The current data already set strong constraints on the effective interactions in a complementary manner. The constraint from collider searches is most effective at a relatively low mass of DM, and the antiproton-to-proton flux ratio offers the best bound for a heavy DM, while the spin-independent direct detection is the best in between. For DM mass of order 10 GeV to 1 TeV, the effective interaction scale is constrained to be typically above a few tens TeV.

---

\*Electronic address: dingran@mail.nankai.edu.cn

†Electronic address: liaoy@nankai.edu.cn

‡Electronic address: liujy@tjut.edu.cn

§Electronic address: wangkai1@zju.edu.cn

## I. INTRODUCTION

The evidence for the domination of dark matter (DM) over ordinary matter in our universe is robust, but still restricted to its gravitational effects after years of efforts, from Zwicky's suggestion in 1930's to explain the rotation curves of galaxies and galaxy clusters to recent precision measurements on cosmic microwave background; see [1, 2] for brief reviews. If some part of DM is nonbaryonic as data indicated and has the nature of particles, it should interact weakly with ordinary matter to cause other effects that could be observable by the means of particle detection. Indeed, there have been many observational and experimental activities trying to reveal various aspects of DM particles, from direct and indirect detections to collider searches. They have provided useful constraints on the nature of DM particles, and may hopefully discover them in the near future.

Many new physics models contain massive neutral particles whose stability is protected by certain exact or approximate symmetries, and thus could serve as DM particles. Most extensively studied are perhaps supersymmetric models; also popular are models based on extra dimensions [3]-[6], and little-Higgs models [7, 8], to mention a few among many; see [9]-[12] for detailed reviews. Since the basic properties of DM particles are more or less fixed in these models, for instance, their spins, structures and orders of magnitude of interactions with ordinary matter, it is possible to make rather detailed predictions on their observational effects. On the other hand, the physical relevance of the models themselves remains to be experimentally verified. Considering our still limited knowledge on DM particles, it is necessary to avoid theoretical biases in exploring various possibilities. In such a circumstance, the effective field theory approach could be very useful [13]. By assuming basic properties of a DM particle such as its spin and mass, one exhausts its effective interactions with ordinary matter that respect known symmetries and are of leading order at low energies while leaving interaction strengths as phenomenological parameters. The physical effects can then be determined in terms of those parameters and confronted with experimental measurements. If a DM particle is fortunately discovered, the rough information gathered for those properties and parameters could be employed as important physical input in planning future facilities to reveal its underlying dynamics.

The DM candidates of a spin zero, spin-1/2, and spin one particle have been exhaustively studied in the literature in the framework of effective field theory [14]-[30]. Recently, two of us have considered the possibility that the DM particle may have spin-3/2 [31] (see also Ref.

[32] on the same suggestion). In that work, the quantum numbers of the DM particle under the standard model (SM) gauge group were not specified, and the constraints from direct and indirect detection data were found similar to those for a spin-1/2 particle. Since DM interacts very weakly with ordinary matter, it should more naturally be a SM singlet. Here we consider this option and investigate the constraints coming from collider measurements as well as direct and indirect detections. A light, singlet DM particle of spin-3/2 has also been studied earlier [33] in rare decays of the  $K$  and  $B$  mesons where the particle appears as missing energy in final states. While the kinematics of such a particle is similar to that of a gravitino, which is also a DM candidate in supergravity models (see [34] for a review), the interactions to be examined here are very different. A charged spin-3/2 particle was also proposed earlier [35] as a constituent of the so-called dark atoms. More recently, a specific model of a spin-3/2 particle was suggested and its direct detection examined [36], in which the particle is charged under the SM gauge group. The possible relevance of spin-3/2 particles has also been considered in other contexts, see for instance, Ref. [37], on collider effects of a spin-3/2 top partner.

The paper is organized as follows. In the next section we consider possible effective interactions of a singlet, spin-3/2 particle with the standard model particles, and set up our conventions for spin-3/2 particles. This is followed by sec III on the Large Hadron Collider (LHC) effects of DM particles that may appear as missing energy in monojet events. In sections IV and V, we consider, respectively, the direct detection via DM scattering off nuclei and the indirect detection through impacts on the cosmic rays. All of these constraints are combined in sec VI together with that from the observed relic density. We summarize briefly in the last section.

## II. EFFECTIVE INTERACTIONS

The field corresponding to a particle of spin-3/2 and mass  $M$  is described by a vector-spinor,  $\Psi_\mu$ , with the constraint,  $\gamma^\mu \Psi_\mu = 0$  [38]. The free field satisfies the equation of motion,  $(i\partial - M)\Psi_\mu = 0$ . The wavefunction of such a particle with momentum  $p$  and helicity  $\lambda$ ,  $U_\mu(p, \lambda)$ , can be constructed from that of a Dirac particle and the polarization of a spin one particle in terms of the Clebsch-Gordan coefficients [39]. For later applications we will need the polarization sums for such a particle,  $P_{\nu\mu}(p) = \sum_\lambda U_\nu(p, \lambda) \bar{U}_\mu(p, \lambda)$ , and for an antiparticle,  $Q_{\nu\mu}(p) = \sum_\lambda V_\nu(p, \lambda) \bar{V}_\mu(p, \lambda)$ , with  $V_\mu(p, \lambda)$  being the antiparticle's wavefunction. They are

known to be

$$P_{\mu\nu}(p) = -(\not{p} + M) \left( T_{\mu\nu}(p) - \frac{1}{3} \gamma^\rho T_{\rho\mu}(p) T_{\nu\sigma}(p) \gamma^\sigma \right), \quad (1)$$

and  $Q_{\mu\nu}(p) = P_{\mu\nu}(p)|_{M \rightarrow -M}$ , where  $T_{\mu\nu}(p) = g_{\mu\nu} - p_\mu p_\nu / p^2$  and  $p^2 = M^2$ .

We consider the effective interactions of a spin-3/2 particle with the SM fermions,

$$L_L (-1), E_R (-2); Q_L (1/3), U_R (4/3), D_R (-2/3); \quad (2)$$

where the number in parentheses denotes the hypercharge  $Y$  which is related to the electric charge  $Q$  and third weak isospin  $T^3$  by the convention  $Q = T^3 + Y/2$ . We start with the operators that involve a pair of SM fermions and a pair of spin-3/2 fields. Lorentz invariance allows for a list of fourteen independent structures [31] as explicitly verified using the generalized Fierz identities [40]. Demanding  $\Psi_\mu$  to be a SM singlet reduces the list to the following four:

$$\begin{aligned} \mathcal{O}_1^f &= \bar{\Psi}_\mu \gamma^\alpha P_- \Psi^\mu \bar{f}_L \gamma_\alpha f_L, \\ \mathcal{O}_2^f &= \bar{\Psi}_\mu \gamma^\alpha P_+ \Psi^\mu \bar{f}_R \gamma_\alpha f_R, \\ \mathcal{O}_3^f &= \bar{\Psi}_\mu \gamma^\alpha P_- \Psi^\mu \bar{f}_R \gamma_\alpha f_R, \\ \mathcal{O}_4^f &= \bar{\Psi}_\mu \gamma^\alpha P_+ \Psi^\mu \bar{f}_L \gamma_\alpha f_L, \end{aligned} \quad (3)$$

where  $P_\pm = (1 \pm \gamma_5)/2$  and  $f_L$  ( $f_R$ ) refers to any SM doublet (singlet) fermion field. Note that the operators are automatically flavor diagonal and that reshuffling a  $\Psi_\mu$  with an  $f$  does not introduce independent operators according to [40]. The corresponding effective interactions are parameterized as

$$\mathcal{L}_{\text{eff}} = +\Lambda^{-2} \sum_{f=L,Q} (c_1^f \mathcal{O}_1^f + c_4^f \mathcal{O}_4^f) + \Lambda^{-2} \sum_{f=E,U,D} (c_2^f \mathcal{O}_2^f + c_3^f \mathcal{O}_3^f), \quad (4)$$

where  $\Lambda$  is the typical energy scale inducing the interactions and  $c_i^f$ s are dimensionless real parameters presumably of order one. Our later numerical analysis will be based on this effective Lagrangian. To reduce the number of unknowns, we follow the usual practice: we treat one operator at a time and assume a universal  $c^f$  for all relevant SM fermions.

We mention briefly some other operators that can be built out of the spin-3/2 field and the SM fields using the approach in [40]. Each of these operators violates either the lepton or baryon number but not both, and is also forbidden if the DM particle carries certain conserved parity. They could thus be phenomenologically dangerous, and we will study them elsewhere. An operator

involving a single SM fermion requires an odd number of the  $\Psi_\mu$  field. With a single  $\Psi_\mu$ , such an operator has the lowest possible dimension five,  $(D^\mu \tilde{H})^\dagger \bar{\Psi}_\mu L_L$ , plus one constructed with the help of charge conjugation. Here  $H$  is the Higgs doublet with  $\tilde{H} = \varepsilon H^*$ , and  $D^\mu$  is the SM gauge covariant derivative. There is no similar operator involving a quark field. It is not possible either to form a dimension six operator involving a single SM fermion and three  $\Psi_\mu$ s without including a genuinely neutral field of neutrinos,  $\nu_R$ . If  $\nu_R$  is indeed introduced, there are then seven such operators according to the results in [40]. An operator involving three SM fermions contains at least a single  $\Psi_\mu$ , corresponding to a dimension six operator. The situation is a bit complicated since one can have pure-lepton, pure-quark, and mixed lepton-quark operators, involving additional color contraction for the latter two. For simplicity, we show here only the pure-lepton operators. Lorentz invariance allows a complete and independent list of four chirality-diagonal (like  $\mathcal{O}_{1,2}^f$ ) structures and four chirality-flipped (like  $\mathcal{O}_{3,4}^f$ ) ones. But gauge symmetry of SM singles out only the following operators,  $\varepsilon^{ab} \overline{L_{iL}^a} \sigma^{\mu\nu} E_{kR} \overline{L_{jL}^b} \gamma_\nu \Psi_\mu$ ,  $\varepsilon^{ab} (\overline{L_{iL}^a})^C \sigma^{\mu\nu} L_{jL}^b \overline{E_{kR}} \gamma_\nu \Psi_\mu$ , where  $i, j, k$  stand for family and  $a, b$  for the third weak isospin.

### III. DIRECT DM PRODUCTION AT LHC AND ITS CONSTRAINTS

In this section, we study the collider phenomenology of spin-3/2 DM using the effective interactions shown in sec II. Since the DM particle is electrically and chromatically neutral, it is completely invisible for detectors and only appears as missing transverse energy ( $\cancel{E}_T$ ) at LHC. The direct production of DM pairs would then be completely invisible with nothing to trigger on. For the trigger purpose, we could focus on the production of a DM pair in association with an initial state radiation jet or photon. In the case of a monojet plus  $\cancel{E}_T$  final state, the level one trigger requires that the sum of the jet transverse momentum ( $p_T^j$ ) and missing transverse energy,  $p_T^j + \cancel{E}_T$ , be greater than 250 GeV or so at the LHC detectors. Studies on monojet signatures with spin-1/2 DM effective operators have been performed extensively [24, 41–47]. Here, we use the latest data on search of monojet final states to constrain the effective interactions involving spin-3/2 DM.

There are three independent subprocesses for production of a monojet plus a DM pair,

$$q\bar{q} \rightarrow g \Psi_\mu \bar{\Psi}_\nu \quad \text{and} \quad gq(\bar{q}) \rightarrow q(\bar{q}) \Psi_\mu \bar{\Psi}_\nu, \quad (5)$$

corresponding to Feynman diagrams in Fig. 1, where  $g$  stands for a gluon. We compute in the appendix the spin- and color-summed and -averaged matrix elements squared due to various op-

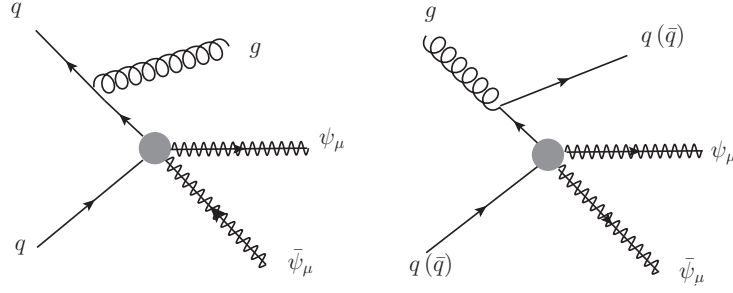


FIG. 1: Feynman diagrams for a monojet plus a spin-3/2 DM pair production at a hadron collider.

erators  $\mathcal{O}_i$ . To illustrate the feature, we show here the result for the subprocess  $q(p_1)\bar{q}(p_2) \rightarrow g(k_j)\Psi_\mu(k_1)\bar{\Psi}_\nu(k_2)$  due to the operator  $\mathcal{O}_1$ , i.e., assuming  $c_1 = 1$  and  $c_{2,3,4} = 0$ ,

$$\sum |\overline{\mathcal{A}}|^2 = \frac{g_s^2}{9\Lambda^4} \frac{8}{9M^4 x_1 x_2} B. \quad (6)$$

Here  $g_s$  is the QCD gauge coupling, and assuming massless quarks, one has,

$$\begin{aligned} B = & \left[ 4M^6(1-x_1)^2 + 2M^4 s(1-x_1-x_2)(1-x_1-y_1)(5-5x_1-7y_1) \right. \\ & \left. - 4M^2 s^2(1-x_1-x_2)^2(1-x_1-y_1)^2 + s^3(1-x_1-x_2)^3(1-x_1-y_1)^2 \right] \\ & + (x_1 \leftrightarrow x_2, y_1 \leftrightarrow y_2), \end{aligned} \quad (7)$$

where  $s = (p_1 + p_2)^2$ , and  $x_i, y_i$  are kinematical variables defined in the appendix. The result due to the operator  $\mathcal{O}_2$  alone is identical. The same degeneracy also occurs between the operators  $\mathcal{O}_3$  and  $\mathcal{O}_4$ , and is due to the spin summation and averaging. Our numerical analysis shows that the difference in angular distributions between the operators  $\mathcal{O}_{1,2}$  on one side and  $\mathcal{O}_{3,4}$  on the other, as the expressions for various  $B$ s indicate, is further smeared out by phase space integration, resulting in the same total cross sections within about one percent. The four operators are thus equivalent for the phenomenology considered here when a universal coupling  $c_i^f$  is assumed, and from now on we will denote them simply by  $\mathcal{O}$ . Compared to the case of spin-1/2 DM, the production of spin-3/2 DM is enhanced in the low mass or high energy region, and we thus expect more stringent bounds could be set in this case.

In Fig. 2 we show the numerical result for the total cross section of a monojet plus  $\cancel{E}_T$  due to any one operator  $\mathcal{O}$  at 7 TeV LHC using different jet  $p_T$  cuts. The effective scale  $\Lambda$  is fixed at

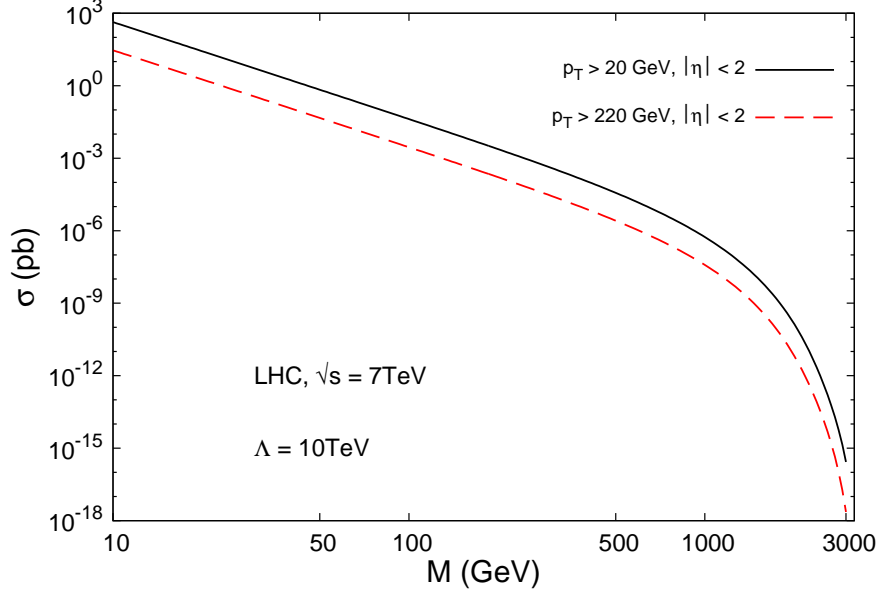


FIG. 2: Total partonic cross section of direct production of a DM pair plus a monojet at 7 TeV LHC as a function of DM mass for any one operator  $\mathcal{O}$ . We choose the PDF set CTEQ6L1 with renormalization scale  $\mu_R = Q$  and factorization scale  $\mu_F = Q/2$ , and  $\Lambda = 10$  TeV.

10 TeV, and we choose the parton distribution function (PDF) set CTEQ6L1 [48], with renormalization scale  $\mu_R = Q$  and factorization scale  $\mu_F = Q/2$ . The monojet cut is within  $|\eta|_j < 2$  with  $p_T^j > 20$  GeV and  $p_T^j > 220$  GeV respectively. The cross section is dominated in the high energy region by the  $s^3$  terms in the amplitude squared; only when the DM mass becomes non-negligible compared with  $\sqrt{s}$ , does the phase space suppression begin to play a significant role and reduce the cross section rapidly. This is reminiscent of the well-known gravitino-goldstino equivalence in supergravity models [49–51]. In the high energy limit, the polarization sum  $P_{\mu\nu}(p)$  approaches  $-\not{p}g_{\mu\nu} + 2/(3M^2)\not{p}p_\mu p_\nu$ , where the first and second term can be identified with the helicity states  $\lambda = \pm 3/2$  and  $\lambda = \pm 1/2$  respectively [52]. The dominance of the latter amounts to an effective description by a spin-1/2 field  $\Psi$  via  $\Psi_\mu \rightarrow \sqrt{2/3}M^{-1}\partial_\mu\Psi$  [53, 54]. The results using the full field  $\Psi_\mu$  and its effective description are compared in Fig. 3, where both the cross sections and their ratio are shown. It is clear that the ratio approaches unity in the low  $M$  region and drops when  $M$  increases beyond about 500 GeV.

Recently, both ATLAS [55] and CMS [56] collaborations have released their studies on monojet plus  $\cancel{E}_T$  events based on data at  $\sqrt{s} = 7$  TeV and with an integrated luminosity of  $4.7 \text{ fb}^{-1}$  and  $5.0 \text{ fb}^{-1}$ , respectively. We use these latest data to derive bounds on our effective operators. Since

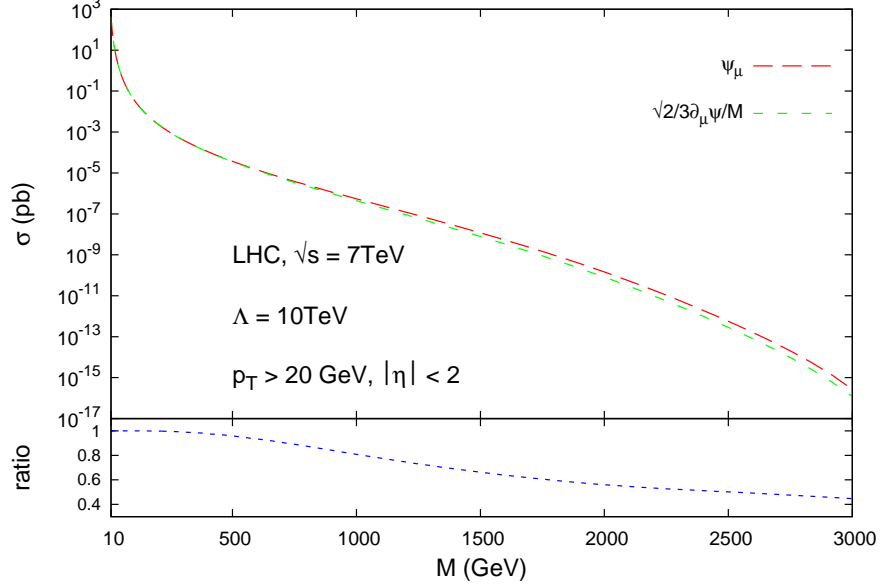


FIG. 3: Total partonic cross section for production of a DM pair plus monojet at 7 TeV LHC is shown as a function of DM mass for operator  $\mathcal{O}$  using the full field  $\Psi_\mu$  or its effective description,  $\sqrt{2/3}M^{-1}\partial_\mu\Psi$ . Also shown is the ratio of results in the two approaches. Same physical input as in Fig. 2.

the monojet  $p_T$  cut is typically required to be harder than 100 GeV, we simulate our signal events with a partonic monojet plus a DM pair without parton showers. In addition, in order to simulate the detector performance at the ATLAS and CMS detectors, we smear jets preformed according to the energy resolution [57, 58]:

$$\begin{aligned}\frac{\Delta E_J}{E_J} &= \frac{0.8}{\sqrt{E_J/\text{GeV}}} \oplus 0.15 \quad \text{for ATLAS,} \\ \frac{\Delta E_J}{E_J} &= \frac{1.0}{\sqrt{E_J/\text{GeV}}} \oplus 0.05 \quad \text{for CMS.}\end{aligned}\tag{8}$$

The SM background is taken from the ATLAS/CMS analysis including the corresponding uncertainties. The QCD jet production in principle can contribute to monojet plus  $\cancel{E}_T$  final states due to the jet energy resolution. However, in this case, the distribution  $d\sigma/d\cancel{E}_T$  drops rapidly before  $\cancel{E}_T < 100$  GeV. The leading SM background then consists of a monojet plus a  $Z$  boson with invisible  $Z$  decays or a monojet plus a  $W^\pm$  boson decaying into soft leptons. Therefore, a large  $\cancel{E}_T$  with a high  $p_T$  monojet typically works as a good selection cut, and as we mentioned, the level one trigger is,  $p_T^j + \cancel{E}_T > 250$  GeV. The ATLAS/CMS searches have assumed four sets of selection cuts, namely, SR1/SR2/SR3/SR4 [55, 56]. In Table I, we summarize the selection cuts and latest data from ATLAS and CMS.



	ATLAS 7TeV, 4.7fb <sup>-1</sup>	CMS 7TeV, 5.0fb <sup>-1</sup>
Signal region	SR1 /SR2 /SR3 /SR4	SR1 /SR2 /SR3 /SR4
$\cancel{E}_T$ (GeV) >	120 /220 /350 /500	250 /300 /350 /400
$p_T^{j_1}$ (GeV) >	120 /220 /350 /500	110
$ \eta _{j_1} <$	2	2.4
$N_{\text{SM}}$	124000 /8800 /750 /83	7842 /2757 /1225 /573
$\sigma_{\text{SM}}$	4000 /400 /60 /14	367 /167 /101 /65
$N_{\text{obs}}$	124703 /8631 /785 /77	7584 /2774 /1142 /522

TABLE I: Crucial cuts and data in the ATLAS [55] and CMS [56] monojet plus  $\cancel{E}_T$  analyses.

To obtain the collider bounds, we follow the  $\chi^2$  definition in Ref. [47]:

$$\chi^2 = \frac{(N(\Lambda, M) + N_{\text{SM}} - N_{\text{obs}})^2}{N_{\text{obs}} + \sigma_{\text{SM}}^2}, \quad (9)$$

where  $N_{\text{SM}}$  is the number of SM background events with the uncertainty  $\sigma_{\text{SM}}$  covering both statistical and systematical uncertainties,  $N_{\text{obs}}$  is the number of observed events, and  $N(\Lambda, M)$  is the event number of DM contribution from an effective operator. Here we require  $\chi^2 = 2.71$  to derive the 90% CL exclusion bounds. Fig. 4 shows the results on the effective scale  $\Lambda$  corresponding to the signal regions from SR1 to SR4, respectively. We note that the plots have a similar shape, namely, exhibit a nearly  $M^{-4}$  slope in the light DM mass region and begin to fall off around  $M > 500$  GeV.

#### IV. DIRECT DETECTION CONSTRAINTS

The direct detection of DM measures the event rate and energy deposit in the collision of target nuclei ( $N$ ) by DM particles ( $\Psi_\mu$ ) in the local halo. It is customary to present the results in terms of the spin-summed and -averaged cross section for the collision at zero momentum transfer:

$$\sigma_0 = \frac{1}{16\pi(M + m_N)^2} \sum_{\text{spins}} |\overline{\mathcal{A}}|^2, \quad (10)$$

where  $\mathcal{A}$  is the scattering amplitude. Nevertheless, the procedure from the ‘microscopic’ interactions in Eq. (4) to the ‘macroscopic’ scattering amplitude is nontrivial. For a nice review on

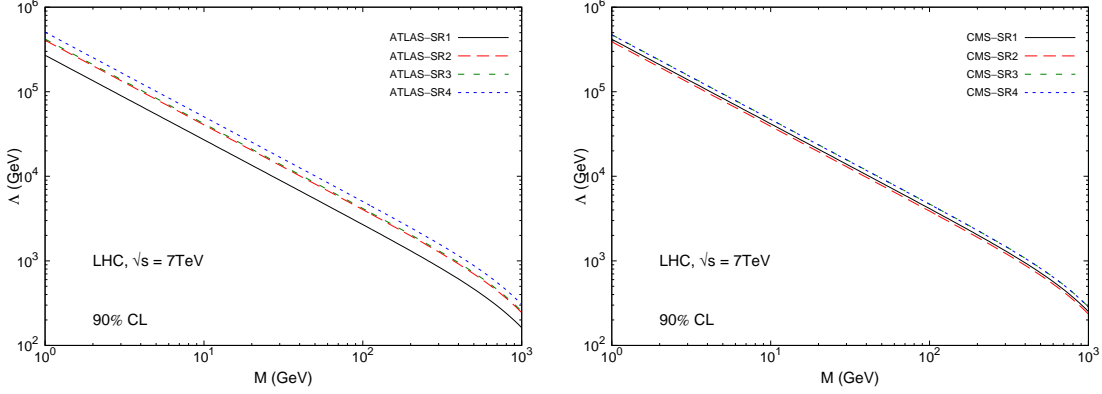


FIG. 4: Lower bounds on  $\Lambda$  set by monojet plus  $\cancel{E}_T$  data from ATLAS [55] (left panel) and CMS [56] (right) experiments. The curves correspond to the signal regions from SR1 to SR4 in table I.

the issue with potential uncertainties incurred, see Ref. [9]; for a summary of the procedure and a detailed analysis of the operators relevant to our discussion here, see Ref. [31]. Since the DM particles are nonrelativistic, they only feel the mass and spin of a nucleus. The collision can thus be classified into the spin-independent (SI) and spin-dependent (SD) ones. Our operators in Eq. (3) are linear compositions of the 9th to 12th operators in [31]. In the nonrelativistic limit, these operators are dominated by the mass-mass and spin-spin terms, i.e., by the structures of  $\gamma^\alpha \otimes \gamma_\alpha$  and  $\gamma^\alpha \gamma_5 \otimes \gamma_\alpha \gamma_5$ , with the parity-mixed terms safely ignorable. They are thus equivalent, and each contributes simultaneously to the SI and SD cross sections:

$$\sigma_0^{\text{SI}} = \frac{\mu^2}{\pi} (b_N)^2, \quad (11)$$

$$\sigma_0^{\text{SD}} = \frac{\mu^2}{\pi} J_N(J_N + 1) (g_N)^2 \frac{20}{3}, \quad (12)$$

with  $\mu = m_N M / (m_N + M)$  being the reduced mass of the  $\Psi$ - $N$  system. Here the effective coupling  $b_N$  essentially accounts for the contributions of valence quarks of nucleons in a nucleus of mass number  $A$  and charge  $Z$ :

$$b_N = Z b_p + (A - Z) b_n, \quad b_p = \Lambda^{-2} (2c^u + c^d), \quad b_n = \Lambda^{-2} (c^u + 2c^d). \quad (13)$$

The effective coupling  $g_N$  can also be decomposed into a sum of contributions in a nucleus of total spin  $J_N$ :

$$g_N = \Lambda^{-2} \sum_q c^q \lambda_q^N, \quad \lambda_q^N = J_N^{-1} [\langle S_p \rangle \Delta_q^p + \langle S_n \rangle \Delta_q^n], \quad (14)$$

where  $\Delta_q^{p(n)}$  is the fraction of the proton (neutron) spin carried by the quark  $q$  [59],  $\langle S_p \rangle$  and  $\langle S_n \rangle$  are the expectation values of the total spin of protons and neutrons. When we consider the DM-proton (neutron) cross section, we have  $\langle S_{p(n)} \rangle = 1/2$  and  $J_N = 1/2$ . For  $\Delta_q^{p(n)}$ , we use the values in Ref. [18]:  $\Delta_u^p = \Delta_d^n = 0.78 \pm 0.02$ ,  $\Delta_d^p = \Delta_u^n = -0.48 \pm 0.02$ , and  $\Delta_s^p = \Delta_s^n = -0.15 \pm 0.02$ . Combining Eqs. (11,12), we get for any one of the operators in Eq. (3),

$$\sigma_0^{\mathcal{O}} = \frac{\mu^2}{4\pi} [(b_N)^2 + \frac{20}{3} J_N(J_N + 1)(g_N)^2]. \quad (15)$$

There exist tensions among current experimental results. Both DAMA [60] and CoGENT [61] experiments claimed to have observed a positive signal, consistent with a DM particle of mass 10 GeV and spin-independent cross section  $\sigma_{\text{SI}} \sim 2 \times 10^{-40} \text{ cm}^2$  and  $\sigma_{\text{SI}} \sim 7 \times 10^{-41} \text{ cm}^2$ , respectively. On the contrary, XENON [62, 63], CDMS [64, 65] and other experiments reported negative results. We do not consider the DAMA and CoGENT results in this paper, because one would need some isospin-violating DM model to compromise with other experiments in a consistent way.

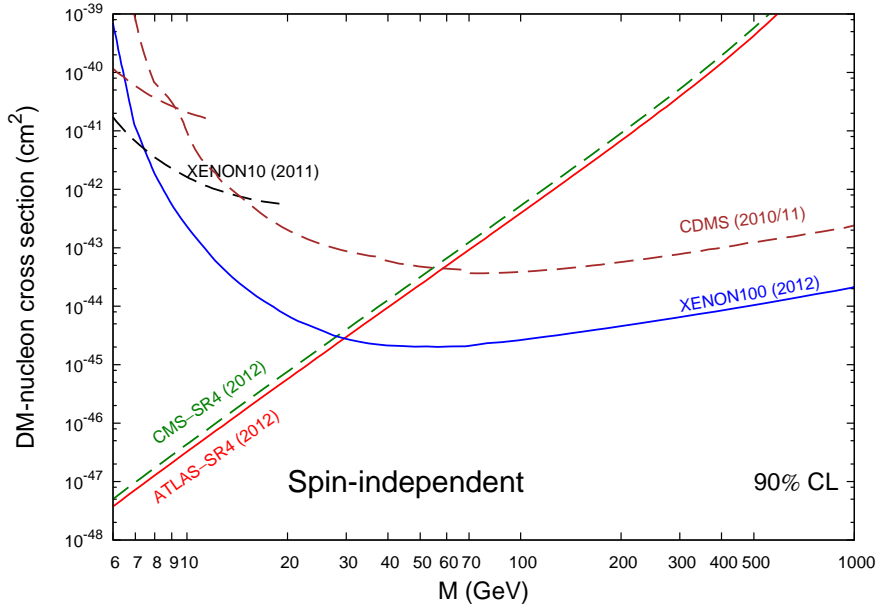


FIG. 5: 90% CL upper limits inferred by ATLAS and CMS limits on SI DM-nucleon cross section as a function of mass  $M$ . Also shown are 90% CL limits from the XENON100 [62], XENON10 [63], and CDMSII [64, 65] experiments.

We present upper limits inferred by the ATLAS and CMS 90% CL limits on the SI and SD cross sections in Figs. 5 and 6 respectively. For comparison, the exclusion curves from various direct detection experiments are also depicted; see the captions for the detail. As one can see from the

figures, SD detections generally set a weaker bound than the LHC searches, while SI detections can yield stronger constraints than the LHC searches for a relatively large DM mass, similarly to the case of a spin-1/2 DM particle. However, for a light DM particle of spin-3/2, the LHC already sets a much more stringent bound than the direct detections. This is in sharp contrast to the case of a spin-1/2 DM particle, and originates from the enhancement discussed in sec III.

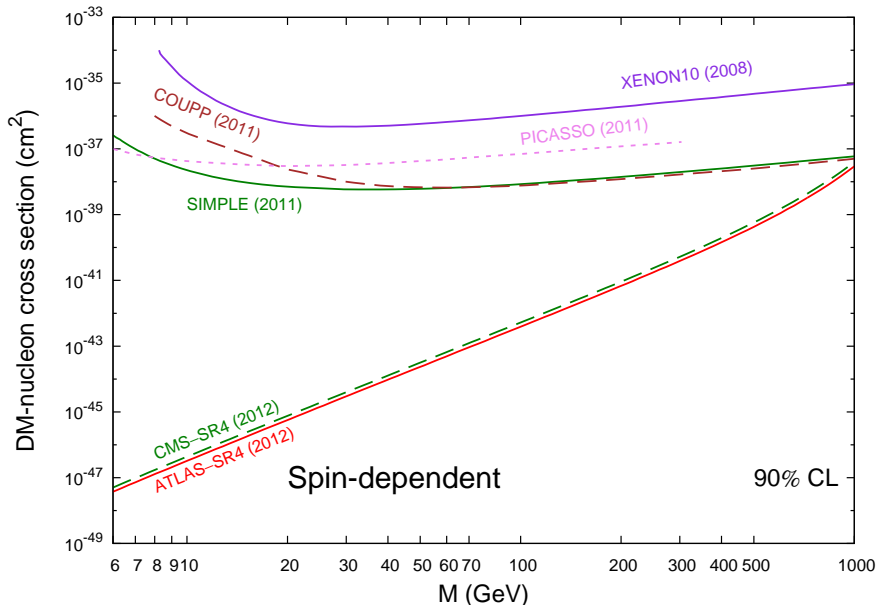


FIG. 6: 90% upper limits inferred by ATLAS and CMS limits on SD DM-nucleon scattering as a function of mass  $M$ . Also shown are 90% CL limits from the SIMPLE [66], COUPP [67], Picasso [68], and XENON10 [69] experiments.

## V. INDIRECT DETECTION CONSTRAINTS

When the DM particles in our Galaxy annihilate, they produce leptons and quarks which interact further with the interstellar medium to initiate more secondary particles, including gamma rays, neutrinos, positrons, antiprotons, etc. This provides an additional source of cosmic rays on top of the known ones. Using the observed data on the fluxes of cosmic rays, it is then possible to constrain the DM annihilation rates. In this section, we employ the Fermi-LAT data on the mid-latitude ( $10^\circ < |b| < 20^\circ$ ,  $0^\circ < l < 360^\circ$ )  $\gamma$ -rays [70] and PAMELA data on the antiproton-to-proton flux ratio  $\bar{p}/p$  [71] to constrain our effective interactions.

### A. Diffuse $\gamma$ -rays and antiproton background estimation

Gamma rays play an important role in indirect searches. As they are not deflected by galactic magnetic fields, they point back to their genuine sources. Several mechanisms may be responsible for the galactic diffuse gamma ray backgrounds: decays of  $\pi^0$  mesons produced in nuclear interactions between cosmic rays and the nuclei in interstellar medium, inverse Compton scattering (IC) of electrons off photons and bremsstrahlung from electrons in the Coulomb field of nuclei [72]. In addition to the galactic background, one also expects a contribution from the extragalactic background (EGRB). The sources of these gamma rays include other galaxies, unresolved point sources, large scale structures and interactions between ultra-high energy cosmic rays and CMB photons. Since each of them has different properties, it is difficult to predict the shape and magnitude of EGRB. Observationally, the EGRB can be obtained by subtraction from the data.

The positrons and antiprotons are also important indicators of DM, because they are relatively rare in the galactic environment. As they traverse the interstellar space, they propagate randomly under the influence of galactic magnetic fields, and lose energy through processes of IC and synchrotron radiation [10]. This process may be described by a complicated diffusion equation. The charged particles traversing the solar system are also affected by the solar wind, which results in a shift in the spectrum observed at the Earth compared to the interstellar one. For this, the solar modulation potential is taken as a free parameter ranging from 300 to 1000 MV [73, 74].

A good approach to estimate the spectra of the above cosmic rays is offered by the GALPROP code [75]. It parameterizes the gas densities, nuclear cross sections and energy spectra for different processes, and then solves the diffusion equation numerically to get a complete solution for the density map of all primary and secondary nuclei. We have therefore used GALPROP to calculate both background and DM annihilation components in cosmic rays.

For the galactic diffuse  $\gamma$ -rays background, we calculate various contributions and fit the Fermi-LAT EGRB data with a power-law spectrum,  $E^2 d\Phi/dE = \Phi_0 (E/\text{GeV})^{-\gamma}$ . In calculating the antiproton galactic background, we scan the solar modulation potential to find out that the minimal  $\chi^2$  is reached for the PAMELA  $\bar{p}/p$  data at a value of 330 MV. The results are presented in Fig. 7, together with the  $\chi^2$  corresponding to Fermi-LAT  $\gamma$ -rays and PAMELA  $\bar{p}/p$  flux ratio data.

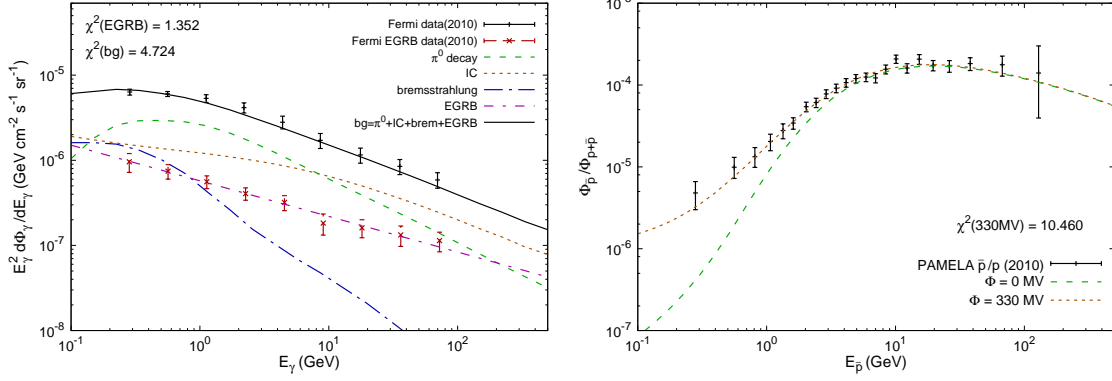


FIG. 7: Left panel: Background estimation for Fermi-LAT  $\gamma$ -ray flux including various contributions and EGRB. The EGRB component is obtained by fitting Fermi-LAT EGRB data with a power-law spectrum. The background flux (dark solid line) is obtained by adding all contributions. Right panel: Background estimation for PAMELA  $\bar{p}/p$  flux ratio. The green dashed (orange short-dashed) line corresponds to the flux without solar modulation (with a solar modulation potential of 330 MV).

## B. Fermi-LAT and PAMELA bounds

Now we derive indirect detection bounds using the Fermi-LAT mid-latitude  $\gamma$ -rays and PAMELA  $\bar{p}/p$  flux ratio data. As before, we treat one operator at a time. It turns out that each of the four operators  $\mathcal{O}_i$  contributes the same to the spin-summed and -averaged total cross section for the annihilation process  $\Psi\bar{\Psi} \rightarrow f\bar{f}$ ,

$$\sigma^f = N^f \frac{s}{16\pi\Lambda^4} \sqrt{\frac{s-4m_f^2}{s-4M^2}} A^f. \quad (16)$$

Here  $s$  is the center-of-mass energy squared,  $m_f$  and  $M$  are respectively the masses of the final ( $f$ ) and initial ( $\Psi$ ) particles, and  $N^f = 1$  (3) when  $f$  is a lepton (quark). We have set one  $c^f$  to unity and others to zero.  $A^f$  is a dimensionless function,

$$A^f = \frac{1}{9} - \frac{r}{6} + \frac{1}{108R^2} - \frac{r}{108R^2} - \frac{5}{108R} + \frac{2r}{27R} - \frac{R}{54} + \frac{8rR}{27}, \quad (17)$$

with  $r = m_f^2/s$  and  $R = M^2/s$ . From Eqs. (16,17), one calculates the thermally averaged annihilation cross section  $\langle\sigma|v|\rangle$  to be

$$\langle\sigma|v|\rangle = \frac{1}{16\pi\Lambda^4} \sum_f N_f \sqrt{1 - \frac{m_f^2}{M^2}} \left( \frac{1}{9} (5M^2 + m_f^2) + \frac{50M^4 - 49M^2m_f^2 + 17m_f^4}{216(M^2 - m_f^2)} \langle v^2 \rangle \right), \quad (18)$$

where  $v$  is the relative velocity of the annihilating DM particles, and the average is over the DM velocity distribution in the particular physical processes considered.

The primary particles (quarks and leptons in our case) from DM annihilation will generate secondary particles (photons and antiprotons) at the production point via parton showers and hadronization. These processes can be simulated by Monte Carlo programs. For a given DM mass from 5 TeV to 10 TeV, we use PYTHIA6.4 [76] to simulate  $dN_\gamma^f/dE_\gamma$  and  $dN_{\bar{p}}^f/dE_{\bar{p}}$ . Here  $dN_\gamma^f/dE_\gamma$  is the energy spectrum of photons produced per annihilation into the final state  $f$ , and  $dN_{\bar{p}}^f/dE_{\bar{p}}$  is that of antiprotons. We considered the  $\Psi\bar{\Psi} \rightarrow q\bar{q}, \ell\bar{\ell}$  channels for the photon spectrum simulation, and  $\Psi\bar{\Psi} \rightarrow q\bar{q}$  for the antiproton. To ensure the accuracy, we took  $10^6$  events in simulation.

The photon flux in a given region  $\Delta\Omega$  due to Dirac-type DM annihilation, is written as [77]

$$\frac{d\Phi_\gamma}{dE_\gamma} = \frac{1}{4\pi} \frac{\bar{J}\Delta\Omega}{4M^2} \sum_f \langle \sigma|v| \rangle_f \frac{dN_\gamma^f}{dE_\gamma}, \quad \bar{J} = \int_{\Delta\Omega} d\Omega(b, l) \int_{\text{l.o.s}} ds \rho_{\text{halo}}^2(r(s, \theta)), \quad (19)$$

where  $f$  runs over all quark and lepton channels.  $r(s, \theta) = (r_\odot^2 + s^2 - 2r_\odot s \cos \theta)^{1/2}$  is the galactic coordinate,  $r_\odot$  the distance of the Sun to the galactic center,  $\theta$  the angle between directions of observation and galactic center, and  $s$  the line of sight (l.o.s) distance. In terms of the galactic latitude  $b$  and longitude  $l$ , one has  $\cos \theta = \cos b \cos l$ . We set the integral region in  $\bar{J}$  to be the Fermi-LAT mid-latitude region ( $10^\circ < |b| < 20^\circ$ ,  $0^\circ < l < 360^\circ$ ). In our calculation, we assume the NFW profile [78]:

$$\frac{\rho_{\text{halo}}(r)}{\rho_\odot} = \frac{r_\odot}{r} \left[ \frac{1 + r_\odot/R}{1 + r/R} \right]^2, \quad (20)$$

where  $\rho_\odot$  is the DM density at the solar location, and  $R$  the scale radius. We adopt the following values for these parameters:  $\rho_\odot = 0.3 \text{ GeV cm}^{-3}$ ,  $r_\odot = 8.33 \text{ kpc}$ , and  $R = 20 \text{ kpc}$ . The galactic DM particles should follow the Maxwell-Boltzmann velocity distribution. We choose the velocity dispersion  $\bar{v} = \sqrt{\langle v^2(r_\odot) \rangle} = \sqrt{3/2} v_c(r_\odot)$ , with  $v_c(r_\odot) = 220 \text{ kms}^{-1}$  being the local circular velocity, and thus  $\langle v^2 \rangle = 2\sqrt{\langle v^2(r_\odot) \rangle}$ . For antiprotons, the source term is

$$Q_{\bar{p}}(r, E) = \frac{1}{4M^2} \rho_{\text{halo}}^2(r) \sum_q \langle \sigma|v| \rangle_q \frac{dN_{\bar{p}}^q}{dE_{\bar{p}}}, \quad (21)$$

where  $q$  runs over all quark channels. We then implement Eqs. (19,21) into GALPROP to calculate the photon flux and  $\bar{p}/p$  flux ratio with the same parameters in background estimation.

To obtain the exclusion bounds, we adopt a simple statistical measurement in Ref. [79]. Adding the DM component with the background flux to get the total flux,  $\Phi_{\text{total}} = \Phi_{\text{bkgd}} + \Phi_{\text{DM}}$ , we define

the difference  $\Delta\chi^2 = \chi_{\text{total}}^2(M, \langle\sigma|v|\rangle) - \chi_{\text{min}}^2$ , where  $\chi_{\text{total}}^2(M, \langle\sigma|v|\rangle)$  is the  $\chi^2$  of the total flux and  $\chi_{\text{min}}^2$  that of the background. The 90% CL limits are then obtained by requiring  $\Delta\chi^2 = 2.71$ . Fig. 8 shows 90% CL limits on the thermally averaged cross section  $\langle\sigma|v|\rangle$  from the Fermi-LAT  $\gamma$ -rays and PAMELA  $\bar{p}/p$  flux ratio data. For comparison, the upper limits from the ATLAS-SR4 and CMS-SR4 are also shown.

There exist another  $\gamma$ -ray limits based on the Fermi-LAT observation of Milky Way dwarf spheroidal satellite galaxies (dSphs) [80]. By a joint likelihood analysis to 10 dSphs with 24 months of Fermi-LAT data, those authors obtained the 95% CL upper limits on (Majorana-type) DM annihilation cross sections for several channels for a DM mass from 5 GeV to 1 TeV, assuming DM couples only to one channel at a time. They are about  $10^{-26} - 6.5 \times 10^{-25} \text{cm}^3 \text{s}^{-1}$  for the  $b\bar{b}$  channel,  $8.4 \times 10^{-26} - 5 \times 10^{-23} \text{cm}^3 \text{s}^{-1}$  for  $\mu^+\mu^-$ , and  $1.4 \times 10^{-26} - 10^{-23} \text{cm}^3 \text{s}^{-1}$  for  $\tau^+\tau^-$ . Upon multiplying them by a factor of two to convert to the case of Dirac-type DM, these limits should be compared to ours on the total cross section which has been obtained assuming that DM couples simultaneously and equally to all possible channels. Their most stringent limit in the  $b\bar{b}$  channel is comparable to our PAMELA  $\bar{p}/p$  limit, while their limits in the lepton channels  $\mu^+\mu^-$  and  $\tau^+\tau^-$  are comparable to our Fermi-LAT limits but less stringent than our PAMELA  $\bar{p}/p$  limit. One could also use the PAMELA positron fraction excess [81] to constrain the annihilation cross section. However, it has been suggested that the excess might arise from some astrophysical sources that were not accounted for earlier, leaving the origin of excess still unclear so far [82, 83].

## VI. COMBINED CONSTRAINTS

In the last sections we studied the individual constraints on DM interactions coming from LHC searches, direct and indirect detections. In this section, we put them together with the constraint from the DM relic density.

The currently observed relic density is a remnant of DM production and annihilation in earlier epochs of our universe. If the annihilation was too fast, there would be not much DM left nowadays; and in the opposite case, DM would be over dense in the current epoch. The observed value can therefore set a constraint on the DM interactions responsible for annihilation. We apply the standard procedure to calculate the relic density [84, 85], i.e., by solving the Boltzmann equation numerically with the annihilation cross section in Eq. (16), summed over all fermions.

In Fig. 9 we present the combined constraints for any one operator  $\mathcal{O}$  for DM mass from



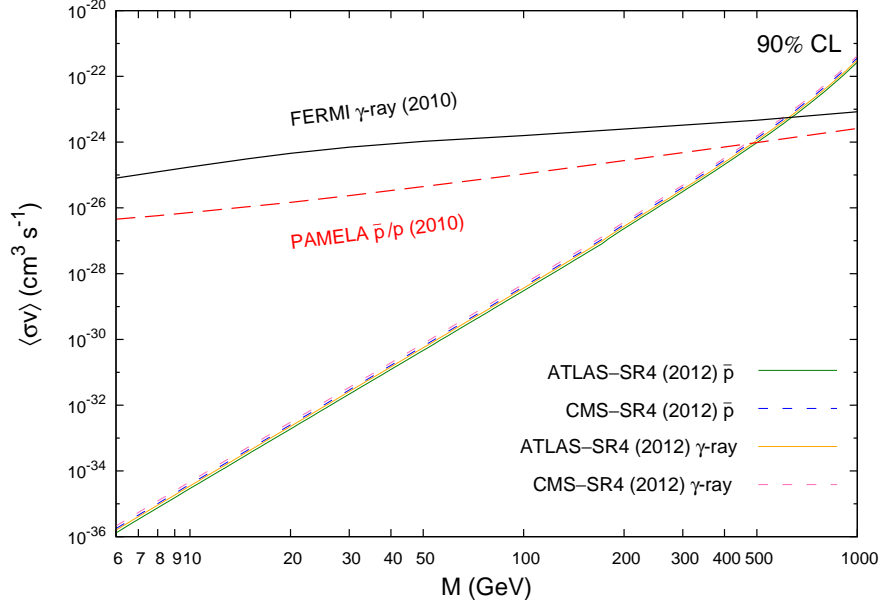


FIG. 8: 90% CL upper limits inferred by Fermi-LAT  $\gamma$ -rays and PAMELA  $\bar{p}/p$  flux ratio on DM annihilation cross section as a function of mass  $M$ . For comparison, 90% CL limits by ATLAS and CMS experiments are also shown.

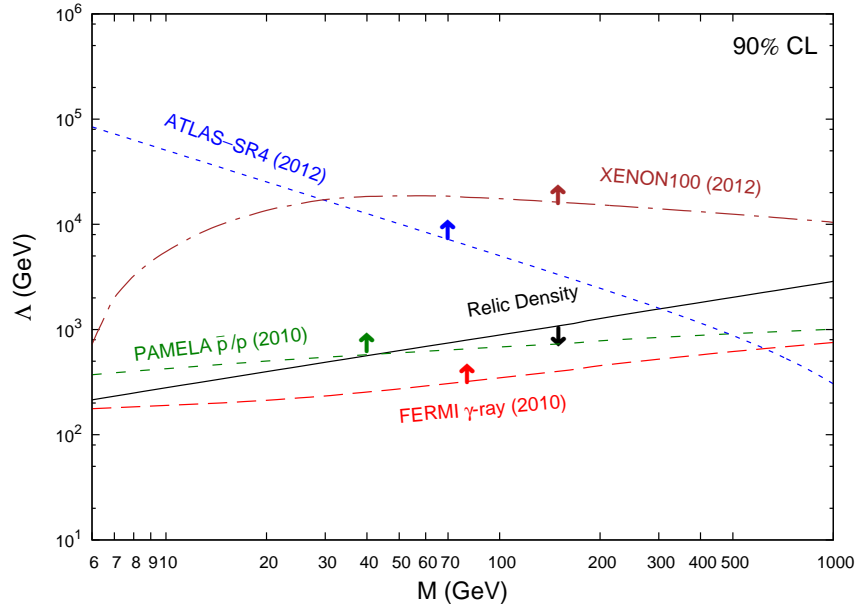


FIG. 9: Combined constraints on the effective scale  $\Lambda$  versus DM mass from 6 GeV to 1 TeV, including observed relic density, ATLAS experiment, SI XENON100 direct detection, Fermi-LAT mid-latitude  $\gamma$ -rays data and PAMELA  $\bar{p}/p$  flux ratio data. The relic density bound is fixed by WMAP7+BAO+ $H_0$  best-fit value, while all other bounds correspond to 90% lower limits.

6 GeV to 1 TeV. All limits correspond to 90% CL except that the relic density is fixed at WMAP7+BAO+ $H_0$  best-fit value,  $\Omega_{\text{DM}}h^2 = 0.1123 \pm 0.0035$  [86]. With one species of DM, the latter would fix the effective scale  $\Lambda$  as a function of  $M$ . If instead one assumes that the particle under consideration is only one of the DM species in the universe, the relic density will set an upper bound on  $\Lambda$ . This is in contrast with all others which set lower limits. For light DM, LHC provides the most stringent constraint, while in the DM mass region from 30 GeV to 1 TeV, the SI direct detection by XENON100 is most restrictive.

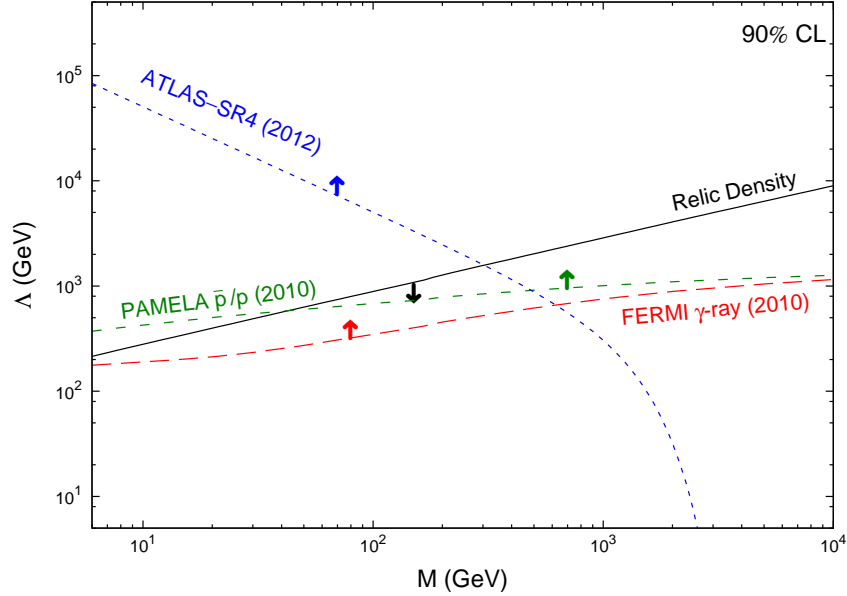


FIG. 10: Similar to Fig. 9, but for DM mass from 6 GeV to 10 TeV.

There is no direct detection constraint when the DM mass is larger than 1 TeV. However, one can still have collider and indirect detection constraints. In Fig. 10, we show the combined constraints from the relic density, LHC searches and indirect detections for DM mass from 6 GeV to 10 TeV. The largest DM mass corresponding to the ATLAS limits is set to be 3 TeV. We find that in the region  $M > 1$  TeV, the PAMELA  $\bar{p}/p$  flux ratio is most stringent. In the LHC searches, as we discussed in sec III, the cross section falls off rapidly in this mass region, resulting in very weak bounds on  $\Lambda$ . However, as the center of mass energy  $\sqrt{s}$  increases, the fall-off will shift to even larger  $M$ . We therefore expect that LHC running at the projected energy of 14 TeV will be capable of pushing the bound on  $\Lambda$  further to higher values.

## VII. CONCLUSION

We have made a comprehensive analysis on the proposal that DM is composed of a spin-3/2 particle which is a singlet of SM. Assuming certain kind of parity for such a particle or assuming the lepton and baryon numbers are still conserved, its leading effective interactions with ordinary particles would involve a pair of them and a pair of SM fermions. Demanding it to be a singlet turns out to be rather restrictive. There are only four types of effective operators in the form of products of chiral currents; and furthermore, all of them have the same or very close phenomenological effects thus simplifying significantly the physical analysis.

Based on the above effective interactions we have investigated DM effects in various experiments and observations. These include the collider searches at LHC for monojet plus missing transverse energy events, direct detections by spin-independent and -dependent scattering off nuclei, indirect detections via observations on  $\gamma$ -rays and antiproton-to-proton flux ratio in cosmic rays, and the relic density. We found that the current data already set strong and complementary constraints. For a relatively light DM particle, say, below 30 GeV, where the DM pair production is much enhanced, the LHC experiments provide very stringent bounds. For instance, the latest data by ATLAS-7 TeV with an integrated luminosity of  $4.7 \text{ fb}^{-1}$  restricts the effective interaction scale to be above 15 TeV to 100 TeV for a dark matter mass of 20 GeV or so. The spin-independent detection by XENON100, on the other hand, offers the most severe constraint for the mass range between 30 GeV and 1 TeV, where the effective scale is required to be above about 20 TeV. Relatively less severely constrained is the heavy DM scenario. For DM mass of 1-3 TeV, the strongest bound comes from the antiproton-to-proton flux ratio in cosmic rays, which excludes effective interactions with an effective scale lower than TeV.

### Acknowledgement

RD would like to thank the members of Zhejiang Institute of Modern Physics for hospitality during a visit when the work was in progress. RD and YL are supported in part by the grant NSFC-11025525 and The Fundamental Research Funds for the Central Universities No.65030021. JYL is supported in part by the grant NSFC-11205113. KW is supported in part by the Zhejiang University Fundamental Research Funds for the Central Universities No.2011QNA3017 and the grants NSFC-11245002, NSFC-11275168.

## Appendix: Amplitudes squared for subprocesses of dark matter pair production plus a monojet

We list here the spin- and color-summed and -averaged amplitudes squared for the subprocesses studied in sec III. They were used as the input file in our numerical simulation code. Denoting the momenta of the initial-state partons, the outgoing parton and the DM particles by  $p_{1,2}$ ,  $k_j$ , and  $k_{1,2}$  respectively, we define the kinematical variables

$$2p_a \cdot k_j = sx_a, \quad 2p_b \cdot k_b = sy_b, \quad (22)$$

where  $s = (p_1 + p_2)^2$ ,  $a, b$  assume values 1, 2, and  $j$  refers to jet. Ignoring parton masses and using  $k_{1,2}^2 = M^2$ , we can express other scalar products of momenta in terms of the variables,

$$\begin{aligned} 2p_1 \cdot k_2 &= (1 - x_1 - y_1)s, \quad 2p_2 \cdot k_1 = (1 - x_2 - y_2)s, \\ 2k_1 \cdot k_j &= (x_1 + y_1 - y_2)s, \quad 2k_2 \cdot k_j = (x_2 - y_1 + y_2)s, \\ 2k_1 \cdot k_2 &= (1 - x_1 - x_2)s - 2M^2. \end{aligned} \quad (23)$$

For the sub-process  $q(p_1)\bar{q}(p_2) \rightarrow g(k_j)\Psi_\mu(k_1)\bar{\Psi}_\nu(k_2)$ , the amplitude squared is given in Eq. (6), where, for either of the operators  $\mathcal{O}_{1,2}$ ,  $B$  is given in Eq. (7), and for either of  $\mathcal{O}_{3,4}$ ,

$$\begin{aligned} B = & \left[ 4M^6(1 - x_1)^2 + 2M^4s(1 - x_1 - x_2)y_1(2x_1 + 7y_1 - 2) \right. \\ & \left. - 4M^2s^2(1 - x_1 - x_2)^2y_1^2 + s^3(1 - x_1 - x_2)^3y_1^2 \right] + (x_1 \leftrightarrow x_2, y_1 \leftrightarrow y_2). \end{aligned} \quad (24)$$

For the sub-process  $q(p_1)g(p_2) \rightarrow q(k_j)\Psi_\mu(k_1)\bar{\Psi}_\nu(k_2)$ , we find

$$\sum |\mathcal{A}|^2 = \frac{g_s^2}{24\Lambda^4} \frac{8}{9M^4x_2} B, \quad (25)$$

where for  $\mathcal{O}_{1,2}$ ,

$$\begin{aligned} B = & 4M^6[(1 - x_1)^2 + (x_1 + x_2)^2] + 2M^4s(1 - x_1 - x_2)(24x_1y_1 - 12x_1y_2 \\ & - 2x_2y_1 + 2x_2y_2 + 10x_1^2 - 2x_2x_1 - 10x_1 + 14y_1^2 + 7y_2^2 - 12y_1 - 14y_1y_2 + 5) \\ & - 4M^2s^2(1 - x_1 - x_2)^2(4x_1y_1 - 2x_1y_2 + 2x_1^2 - 2x_1 + 2y_1^2 + y_2^2 - 2y_1 - 2y_1y_2 + 1) \\ & + s^3(1 - x_1 - x_2)^3(4x_1y_1 - 2x_1y_2 + 2x_1^2 - 2x_1 + 2y_1^2 + y_2^2 - 2y_1 - 2y_1y_2 + 1), \end{aligned} \quad (26)$$

and for  $\mathcal{O}_{3,4}$ ,

$$\begin{aligned} B = & 4M^6[(1 - x_1)^2 + (x_1 + x_2)^2] + 2M^4s(1 - x_1 - x_2)(24x_1y_1 - 12x_1y_2 \\ & - 2x_2y_1 + 2x_2y_2 + 10x_1^2 - 2x_2x_1 - 10x_1 + 14y_1^2 + 7y_2^2 - 12y_1 - 14y_1y_2) \\ & - 4M^2s^2(1 - x_1 - x_2)^2(4x_1y_1 - 2x_1y_2 + 2x_1^2 - 2x_1 + 2y_1^2 + y_2^2 - 2y_1 - 2y_1y_2) \\ & + s^3(1 - x_1 - x_2)^3(-2x_2y_1 + 2x_2y_2 + x_2^2 + 2y_1^2 + y_2^2 - 2y_1y_2). \end{aligned} \quad (27)$$

Finally, the result for the subprocess  $\bar{q}(p_2)g(p_1) \rightarrow \bar{q}(k_j)\Psi_\mu(k_1)\bar{\Psi}_\nu(k_2)$  can be obtained from Eq. (25) by the interchanges,  $x_1 \leftrightarrow x_2$ ,  $y_1 \leftrightarrow y_2$ .

- 
- [1] L. E. Strigari, PATRAS 2010, DESY-PROC-2010-03.
  - [2] A. Berera, *Pramana* **76**, 783 (2011).
  - [3] E. W. Kolb and R. Slansky, *Phys. Lett. B* **135**, 378 (1984).
  - [4] G. Servant and T. M. P. Tait, *Nucl. Phys. B* **650**, 391 (2003) [hep-ph/0206071].
  - [5] H. -C. Cheng, J. L. Feng and K. T. Matchev, *Phys. Rev. Lett.* **89**, 211301 (2002) [hep-ph/0207125].
  - [6] K. Kong and K. T. Matchev, *JHEP* **0601**, 038 (2006) [hep-ph/0509119].
  - [7] H. -C. Cheng and I. Low, *JHEP* **0408**, 061 (2004) [hep-ph/0405243].
  - [8] A. Birkedal, A. Noble, M. Perelstein and A. Spray, *Phys. Rev. D* **74**, 035002 (2006) [hep-ph/0603077].
  - [9] G. Jungman, M. Kamionkowski and K. Griest, *Phys. Rept.* **267**, 195 (1996) [arXiv:hep-ph/9506380].
  - [10] G. Bertone, D. Hooper and J. Silk, *Phys. Rept.* **405**, 279 (2005) [hep-ph/0404175].
  - [11] D. Hooper and S. Profumo, *Phys. Rept.* **453**, 29 (2007) [hep-ph/0701197].
  - [12] J. L. Feng, *Ann. Rev. Astron. Astrophys.* **48**, 495 (2010) [arXiv:1003.0904 [astro-ph.CO]].
  - [13] M. W. Goodman and E. Witten, *Phys. Rev. D* **31**, 3059 (1985).
  - [14] A. Kurylov and M. Kamionkowski, *Phys. Rev. D* **69**, 063503 (2004) [hep-ph/0307185].
  - [15] A. Birkedal, K. Matchev and M. Perelstein, *Phys. Rev. D* **70**, 077701 (2004) [hep-ph/0403004].
  - [16] F. Giuliani, *Phys. Rev. Lett.* **93**, 161301 (2004) [hep-ph/0404010].
  - [17] J. L. Feng, S. Su and F. Takayama, *Phys. Rev. Lett.* **96**, 151802 (2006) [hep-ph/0503117].
  - [18] G. Belanger, F. Boudjema, A. Pukhov and A. Semenov, *Comput. Phys. Commun.* **180**, 747 (2009) [arXiv:0803.2360 [hep-ph]].
  - [19] M. Beltran, D. Hooper, E. W. Kolb and Z. C. Krusberg, *Phys. Rev. D* **80**, 043509 (2009) [arXiv:0808.3384 [hep-ph]].
  - [20] M. Cirelli, M. Kadastik, M. Raidal and A. Strumia, *Nucl. Phys. B* **813**, 1 (2009) [arXiv:0809.2409 [hep-ph]].
  - [21] Q. -H. Cao, C. -R. Chen, C. S. Li and H. Zhang, *JHEP* **1108**, 018 (2011) [arXiv:0912.4511 [hep-ph]].
  - [22] P. Agrawal, Z. Chacko, C. Kilic and R. K. Mishra, arXiv:1003.1912 [hep-ph].
  - [23] J. Fan, M. Reece and L. -T. Wang, *JCAP* **1011**, 042 (2010) [arXiv:1008.1591 [hep-ph]].
  - [24] J. Goodman *et al.*, *Phys. Rev. D* **82**, 116010 (2010) [arXiv:1008.1783 [hep-ph]].

- [25] J. Goodman, M. Ibe, A. Rajaraman, W. Shepherd, T. M. P. Tait and H. -B. Yu, Nucl. Phys. B **844**, 55 (2011) [arXiv:1009.0008 [hep-ph]].
- [26] K. Cheung, K. Mawatari, E. Senaha, P. -Y. Tseng and T. -C. Yuan, JHEP **1010**, 081 (2010) [arXiv:1009.0618 [hep-ph]].
- [27] K. Cheung, P. -Y. Tseng and T. -C. Yuan, JCAP **1101**, 004 (2011) [arXiv:1011.2310 [hep-ph]].
- [28] K. Cheung, P. -Y. Tseng and T. -C. Yuan, JCAP **1106**, 023 (2011) [arXiv:1104.5329 [hep-ph]].
- [29] J. -M. Zheng *et al.*, Nucl. Phys. B **854**, 350 (2012) [arXiv:1012.2022 [hep-ph]].
- [30] M. T. Frandsen, F. Kahlhoefer, S. Sarkar and K. Schmidt-Hoberg, JHEP **1109**, 128 (2011) [arXiv:1107.2118 [hep-ph]].
- [31] R. Ding and Y. Liao, JHEP **1204**, 054 (2012) [arXiv:1201.0506 [hep-ph]].
- [32] Z. -H. Yu, J. -M. Zheng, X. -J. Bi, Z. Li, D. -X. Yao and H. -H. Zhang, Nucl. Phys. B **860**, 115 (2012) [arXiv:1112.6052 [hep-ph]].
- [33] J. F. Kamenik and C. Smith, JHEP **1203**, 090 (2012) [arXiv:1111.6402 [hep-ph]].
- [34] T. Moroi, hep-ph/9503210.
- [35] M. Y. Khlopov, arXiv:0806.3581 [astro-ph]. For a brief review, see: M. Y. Khlopov, Mod. Phys. Lett. A **26**, 2823 (2011) [arXiv:1111.2838 [astro-ph.CO]].
- [36] K. G. Savvidy and J. D. Vergados, arXiv:1211.3214 [hep-ph].
- [37] W. J. Stirling and E. Vryonidou, JHEP **1201**, 055 (2012) [arXiv:1110.1565 [hep-ph]].
- [38] W. Rarita and J. Schwinger, Phys. Rev. **60**, 61 (1941).
- [39] S. Kusaka, Phys. Rev. **60**, 61 (1941).
- [40] Y. Liao and J. -Y. Liu, Eur. Phys. J. Plus **127**, 121 (2012) [arXiv:1206.5141 [hep-ph]].
- [41] M. Beltran, D. Hooper, E. W. Kolb, Z. A. C. Krusberg and T. M. P. Tait, JHEP **1009** (2010) 037 [arXiv:1002.4137 [hep-ph]].
- [42] J. Goodman, M. Ibe, A. Rajaraman, W. Shepherd, T. M. P. Tait and H. -B. Yu, Phys. Lett. B **695** (2011) 185 [arXiv:1005.1286 [hep-ph]].
- [43] A. Rajaraman, W. Shepherd, T. M. P. Tait and A. M. Wijangco, Phys. Rev. D **84** (2011) 095013 [arXiv:1108.1196 [hep-ph]].
- [44] P. J. Fox, R. Harnik, J. Kopp and Y. Tsai, Phys. Rev. D **85** (2012) 056011 [arXiv:1109.4398 [hep-ph]].
- [45] I. M. Shoemaker and L. Vecchi, Phys. Rev. D **86** (2012) 015023 [arXiv:1112.5457 [hep-ph]].
- [46] J. -F. Fortin and T. M. P. Tait, Phys. Rev. D **85** (2012) 063506 [arXiv:1103.3289 [hep-ph]].
- [47] K. Cheung, P. -Y. Tseng, Y. -L. S. Tsai and T. -C. Yuan, JCAP **1205** (2012) 001 [arXiv:1201.3402

- [hep-ph]].
- [48] P. M. Nadolsky, H. -L. Lai, Q. -H. Cao, J. Huston, J. Pumplin, D. Stump, W. -K. Tung, and C. -P. Yuan, Phys. Rev. D **78**, 013004 (2008) [arXiv:0802.0007 [hep-ph]].
  - [49] P. Fayet, Phys. Lett. B **84** (1979) 421.
  - [50] T. E. Clark, T. Lee, S. T. Love and G. -H. Wu, Phys. Rev. D **57** (1998) 5912 [hep-ph/9712353].
  - [51] T. Lee and G. -H. Wu, Phys. Lett. B **447** (1999) 83 [hep-ph/9805512].
  - [52] M. Bolz, A. Brandenburg and W. Buchmuller, Nucl. Phys. B **606** (2001) 518 [Erratum-ibid. B **790** (2008) 336] [hep-ph/0012052].
  - [53] K. Mawatari and Y. Takaesu, Eur. Phys. J. C **71** (2011) 1640 [arXiv:1101.1289 [hep-ph]].
  - [54] K. Hagiwara, K. Mawatari and Y. Takaesu, Eur. Phys. J. C **71** (2011) 1529 [arXiv:1010.4255 [hep-ph]].
  - [55] G. Aad *et al.* [ATLAS Collaboration], arXiv:1210.4491 [hep-ex].
  - [56] S. Chatrchyan *et al.* [CMS Collaboration], JHEP **1209** (2012) 094 [arXiv:1206.5663 [hep-ex]].
  - [57] ATLAS: Detector and physics performance technical design report. Volume 1, CERN-LHCC-99-14.
  - [58] G. L. Bayatian *et al.* [CMS Collaboration], CMS physics: Technical design report, CERN-LHCC-2006-001.
  - [59] For most recent lattice evaluation, see: G. S. Bali *et al.* [QCDSF Collaboration], Phys. Rev. Lett. **108**, 222001 (2012) [arXiv:1112.3354 [hep-lat]].
  - [60] C. Savage, G. Gelmini, P. Gondolo and K. Freese, JCAP **0904** (2009) 010 [arXiv:0808.3607 [astro-ph]].
  - [61] C. E. Aalseth *et al.* [CoGeNT Collaboration], Phys. Rev. Lett. **106** (2011) 131301 [arXiv:1002.4703 [astro-ph.CO]].
  - [62] E. Aprile *et al.* [XENON100 Collaboration], Phys. Rev. Lett. **109** (2012) 181301 [arXiv:1207.5988 [astro-ph.CO]].
  - [63] J. Angle *et al.* [XENON10 Collaboration], Phys. Rev. Lett. **107** (2011) 051301 [arXiv:1104.3088 [astro-ph.CO]].
  - [64] Z. Ahmed *et al.* [CDMS-II Collaboration], Phys. Rev. Lett. **106** (2011) 131302 [arXiv:1011.2482 [astro-ph.CO]].
  - [65] Z. Ahmed *et al.* [CDMS-II Collaboration], Science **327** (2010) 1619 [arXiv:0912.3592 [astro-ph.CO]].
  - [66] M. Felizardo, T. A. Girard, T. Morlat, A. C. Fernandes, A. R. Ramos, J. G. Marques, A. Kling, and J. Puibasset *et al.*, Phys. Rev. Lett. **108** (2012) 201302 [arXiv:1106.3014 [astro-ph.CO]].

- [67] W. H. Lippincott: talk at TAUP-2011 Workshop, Munich, Germany, Sept. 5-9, 2011.
- [68] V. Zacek: talk at TAUP-2011 Workshop, Munich, Germany, Sept. 5-9, 2011.
- [69] J. Angle *et al.* [XENON10 Colla.], Phys. Rev. Lett. **101**, 091301 (2008) [arXiv:0805.2939 [astro-ph]].
- [70] A. A. Abdo *et al.* [Fermi-LAT Collaboration], Phys. Rev. Lett. **104** (2010) 101101 [arXiv:1002.3603 [astro-ph.HE]].
- [71] O. Adriani *et al.* [PAMELA Collaboration], Phys. Rev. Lett. **105** (2010) 121101 [arXiv:1007.0821 [astro-ph.HE]].
- [72] W. de Boer, C. Sander, V. Zhukov, A. V. Gladyshev and D. I. Kazakov, Astron. Astrophys. **444** (2005) 51 [astro-ph/0508617].
- [73] L. J. Gleeson and W. I. Axford, Astrophys. J. **154**, 1011 (1968).
- [74] G. Belanger, F. Boudjema, P. Brun, A. Pukhov, S. Rosier-Lees, P. Salati and A. Semenov, Comput. Phys. Commun. **182**, 842 (2011) [arXiv:1004.1092 [hep-ph]].
- [75] A. W. Strong, I. V. Moskalenko, T. A. Porter, G. Johannesson, E. Orlando and S. W. Digel, arXiv:0907.0559 [astro-ph.HE]. The website for GALPROP is <http://galprop.stanford.edu/>
- [76] T. Sjostrand, S. Mrenna and P. Z. Skands, JHEP **0605** (2006) 026 [hep-ph/0603175].
- [77] M. Cirelli, G. Corcella, A. Hektor, G. Hutsi, M. Kadastik, P. Panci, M. Raidal and F. Sala *et al.*, JCAP **1103** (2011) 051 [Erratum-ibid. **1210** (2012) E01] [arXiv:1012.4515 [hep-ph]].
- [78] J. F. Navarro, C. S. Frenk and S. D. M. White, Astrophys. J. **462**, 563 (1996) [astro-ph/9508025]; Astrophys. J. **490**, 493 (1997) [astro-ph/9611107].
- [79] M. Cirelli, P. Panci and P. D. Serpico, Nucl. Phys. B **840** (2010) 284 [arXiv:0912.0663 [astro-ph.CO]].
- [80] M. Ackermann *et al.* [Fermi-LAT Collaboration], Phys. Rev. Lett. **107** (2011) 241302 [arXiv:1108.3546 [astro-ph.HE]].
- [81] O. Adriani *et al.* [PAMELA Collaboration], Nature **458** (2009) 607 [arXiv:0810.4995 [astro-ph]].
- [82] M. Cirelli, Pramana **79**, 1021 (2012) [arXiv:1202.1454 [hep-ph]].
- [83] For a brief review, see e.g.: X. G. He, Mod. Phys. Lett. A **24**, 2139 (2009) [arXiv:0908.2908 [hep-ph]].
- [84] E.W. Kolb and M.S. Turner, *The Early Universe* (Addison-Wesley, 1990)
- [85] P. Gondolo and G. Gelmini, Nucl. Phys. B **360**, 145 (1991).
- [86] E. Komatsu *et al.* [WMAP Collaboration], Astrophys. J. Suppl. **192**, 18 (2011) [arXiv:1001.4538 [astro-ph.CO]].